JOURNAL OF APPLIED ELECTROCHEMISTRY **26** (1996) 325–336

Influence of carbon monoxide, ethylene, acetylene, allyl alcohol and propargyl alcohol on nickel electrodissolution in aqueous sulfuric acid solution

C. F. ZINOLA*, A. M. CASTRO LUNA, A. J. ARVIA

Instituto de Investigaciones Fisicoquímicas Teóricas y Aplicadas (INIFTA), Universidad Nacional de La Plata, Sucursal 4, Casilla de Correo 16, (1900) La Plata, Argentina

Received 17 May 1995; revised 14 August 1995

The influence of carbon monoxide, ethylene, acetylene, allyl alcohol and propargyl alcohol on nickel electrodissolution in aqueous 0.5 M H_2SO_4 was studied after the adsorption equilibrium of each of these species at a fixed potential and room temperature had been attained. The hindrance of nickel electrodissolution by carbon monoxide is greater than that resulting from double and triple C–C bond compounds at the same concentration in the solution. Corrosion current, corrosion potential, the amount of dissolved nickel at a constant potential and steady hydrogen evolution polarization data combined with voltammetric deconvolution data provide information about the nickel electrodissolution inhibition capability of these substances in acid solution.

1. Introduction

Nickel and Ni-alloy are relatively low cost materials of technical interest in electrochemical energy conversion devices and electrocatalysis. In aqueous environments, nickel is covered by either an electrochemically active hydroxide layer, or a passive NiO layer depending on the solution composition, applied potential and temperature [1, 2]. CO and some organic species added to acid solution act as an inhibitor of nickel electrodissolution over a certain potential range [3–5]. As the mechanism of nickel corrosion and passivation in aqueous solution is already reasonably well-established [1, 2], the study of Ni-additive interactions in the electrochemical environment offers the possibility of either improving or reducing nickel corrosion resistance.

The interaction of additives with metal surfaces in ionic conducting environments may result in the additive molecule being either adsorbed or electroadsorbed as such or dissociatively. For the latter one, different types of adsorbates [6–9] with particular stoichiometries and structures can be formed. For platinum and gold, this type of interaction has been extensively investigated for a number of substances in acid solution [9, 10].

This work refers to the influence of carbon monoxide (CO), ethylene (ET), acetylene (AC), allyl alcohol (AA) and propargyl alcohol (PA) on nickel electrodissolution in aqueous H_2SO_4 followed by potentiodynamic and potentiostatic techniques. The presence of one of these substances in the acid environment modifies, specifically, the nickel corrosion and passivation including the hydrogen evolution reaction (HER). Changes are interpreted mainly by a competitive adsorption of either the additive itself or its electroadsorption products with OH-containing species resulting from water electrochemical reactions on nickel.

2. Experimental details

Experiments were carried out in a conventional electrochemical cell with a flowing solution device (microflux cell) at 25 °C. The following electrodes were used, a Ni wire (0.298 cm^2 in geometric area) as working electrode (we), a Pt plate (ca. 2 cm^2 in geometric area) as counter electrode, and a reversible hydrogen electrode (RHE) as reference.

Deaerated aqueous 0.5 M H_2SO_4 prepared from 98% H_2SO_4 (p.a.) and Millipore-MilliQ® water was employed as the base solution. CO, ET and AC were purified following the procedures recommended in the literature for each substance [11]. The amount of CO, ET and AC added to the base electrolyte corresponded to solubility saturation at 25 °C, that is, 4.5×10^{-4} M for CO, 5×10^{-3} M for ET and 0.44 M for AC [12]. Otherwise, the AA concentration was varied in the range 7×10^{-3} M $\leqslant c_{AA} \leqslant 0.1$ M, and the PA concentration was in the range $5 \times 10^{-3} \leqslant c_{PA} \leqslant 0.44$ M. These solutions were prepared from repeated distilled p.a. chemicals.

Rest potentials (E_{rest}) of nickel were determined in both aqueous 0.5 M H_2SO_4 (blank) and additive-containing 0.5 M H_2SO_4.

A two-step potential routine (E_1 and E_2) was applied to the working electrode in the blank, namely

*Laboratorio de Electroquímica, Facultad de Ciencias, Universidad de la República, Tristán Narvaja 1674, Montevideo, Uruguay.

0021-891X

at $E_1 = 1.0\,V$ for $t_1 = 4\,s$, and $E_2 = -0.1\,V$ for $t_2 = 4\,s$. Subsequently, the potential was stepped to E_{ad}, the so-called adsorption potential, for 5 min, afterwards the base electrolyte was changed by either CO-, ET-, AC-, AA- or PA-containing aqueous 0.5 M H_2SO_4, and once the corresponding adsorption equilibrium had been attained, the solution was replaced again by aqueous 0.5 M H_2SO_4. Then, a positive-going direction potential scan was run from E_{ad} to 1 V at 0.1 V s^{-1} to strip those adsorbed species which might have formed at E_{ad} and to assist nickel electrodissolution and passivation. The value of q_{ox}, the anodic stripping apparent charge density, was then determined.

The corrosion potential (E_{corr}) and the apparent corrosion current density (j_{corr}) were determined from stationary potentiostatic anodic and cathodic polarization curves. The latter also provide information about the HER.

Current transients immediately after the addition of the additive to the base solution by holding the electrode at E_{rest} were also recorded. These experiments allowed us to distinguish whether additive adsorption or electroadsorption took place.

The amount of nickel dissolved by holding the nickel electrode at $E = 0.25\,V$, $E = 0.50\,V$ and $E = 0.80\,V$, for 15 min, was determined by conventional atomic absorption spectroscopy in both the blank and additive-containing solution.

3. Results

3.1. *Rest potentials*

Values of E_{rest} for nickel in different solutions are assembled in Table 1. In all cases, the presence of an additive shifts positively the value of E_{rest}. This effect increases as the additive concentration in solution is increased. The greatest shift is produced by those compounds with a triple C–C bond.

3.2. *Voltammetric and current transient data*

3.2.1. Ni in aqueous 0.5 M H_2SO_4. Previously reported data [1, 2] showed that the voltammogram of nickel in aqueous H_2SO_4 depends on the applied potential routine, solution composition, nickel electrode pretreatment, and temperature. For data comparison these variables were adequately preset.

The voltammogram of nickel in aqueous 0.5 M H_2SO_4 at 0.1 V s^{-1} run from 0 V upwards (Fig. 1(a)) displays a large anodic current contribution involving peak I at 0.24 V, a hump (peak II) at 0.4 V or

Table 1. Values of E_{rest} for Ni in aqueous 0.5 M H_2SO_4 containing different additives at 25 °C

System	E_{rest}/V
Ni/0.5 M H_2SO_4	−0.038
Ni/(CO sat) 0.5 M H_2SO_4	0.018
Ni/(ET sat) 0.5 M H_2SO_4	0.018
Ni/(AA 7×10^{-3} M) 0.5 M H_2SO_4	0.036
Ni/(AA 0.44 M) 0.5 M H_2SO_4	0.082
Ni/(AA 0.10 M) 0.5 M H_2SO_4	0.105
Ni/(AC sat) 0.5 M H_2SO_4	0.288
Ni/(PA 5×10^{-3} M) 0.5 M H_2SO_4	0.100
Ni/(PA 0.44 M) 0.5 M H_2SO_4	0.278

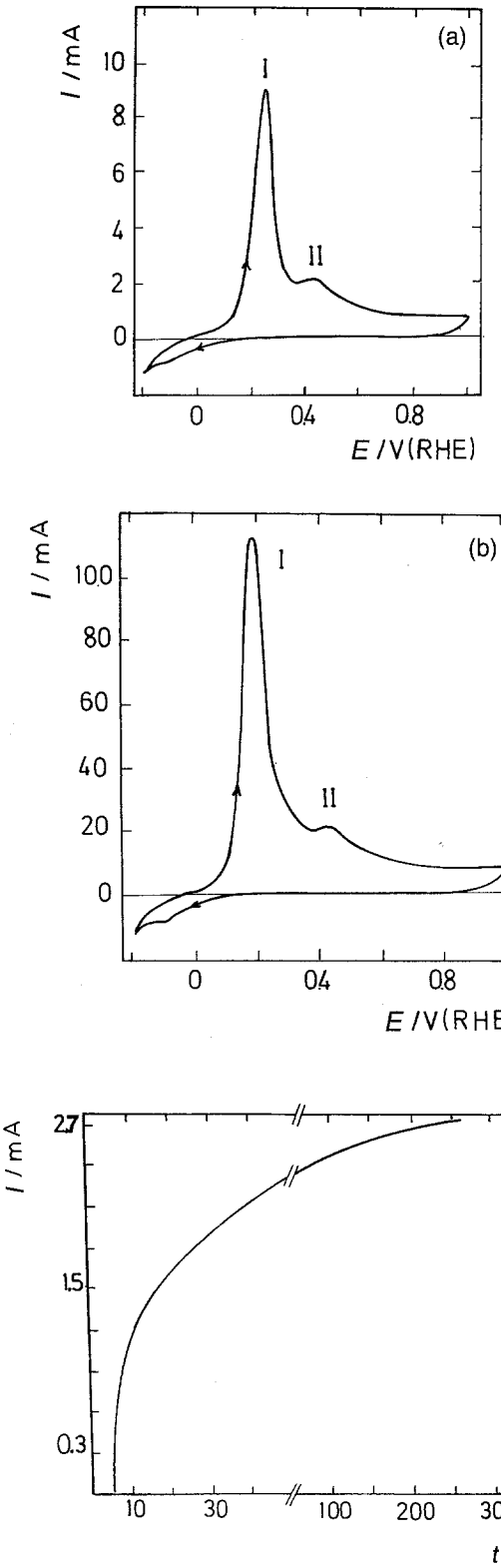

Fig. 1. (a) Cyclic voltammogram for Ni in the blank run at 0.1 V s^{-1}. $T = 25\,°C$. (b) Voltammogram for Ni in the blank after a potential holding at 0 V for 5 min. $v = 0.1\,V\,s^{-1}$, $T = 25\,°C$. (c) Current transient for Ni in the blank run at $E = 0\,V$, $T = 25\,°C$, *we* 0.298 cm^2 in geometric area. The potential sweep direction is indicated by arrows on the voltammograms.

thereabouts, and a passivation current plateau extending from 0.7 to 1 V. The reverse potential scan shows a small cathodic current peak at −0.1 V. On the other hand, a potential holding at 0 V for 5 min produces a considerable enhancement of peak I in the subsequent voltammetric scan (Fig. 1(b)). The value of q_{ox} involved in these experiments is 210 mC cm^{-2} or thereabouts.

Current transients resulting from nickel immersed in the blank by setting E in the range $E_{rest} \leqslant E \leqslant 0.4$ V, show a monotonous increase in anodic current due to nickel electrodissolution (Fig. 1(c)).

3.2.2. Ni in CO-saturated aqueous 0.5 M H_2SO_4. A negligible cathodic current transient for nickel in aqueous 0.5 M H_2SO_4 after CO saturation at either $E = -0.038$ V or $E = 0.018$ V (see Table 1) was observed. Seemingly, in these cases the interaction between Ni and CO in this aqueous environment implies no dominant net charge transfer process.

The voltammogram of nickel in the blank run in the positive potential direction after a 5 min interaction with a CO-containing solution at $E = 0$ V (Fig. 2(a)) shows a remarkable decrease in the height of peak I, and the appearance of a large and sharp anodic current peak at 0.50 V. These voltammograms also show a residual anodic current from 0.8 V upwards overlapping the residual current resulting from the blank. For E in the range $-0.20\,\text{V} \leqslant E \leqslant 0.018$ V, a constant value $q_{ox} \cong 68$ mC cm^{-2} was determined. This value of q_{ox} diminishes for $E > 0.018$ V.

The cyclic voltammogram run after Ni interaction with dissolved CO at 0.1 V s^{-1} between −0.2 and 1 V (Fig. 2(b)), gradually changes in the direction expected for a reactivation of the nickel electrodissolution reaction. After ten cycles the blank voltammogram is approached as the height of peak I increases and exceeds largely that of peak II.

3.2.3. Ni in ET-saturated aqueous 0.5 M H_2SO_4. The same type of experiment referred to in Section 3.2.2 was made in ET-saturated aqueous 0.5 M H_2SO_4. Current transients measured at either $E_{rest} = -0.038$ V or $E_{rest} = 0.018$ V also show a negligible electroadsorption charge.

After Ni interaction with the ET-containing solution, the first voltammogram run from 0 V upwards (Fig. 3(a)) shows a decrease in the height of peak I, and a broad and symmetric peak which is to some extent comparable to peak II in the blank. The value $q_{ox} = 48$ mC cm^{-2} is attained in the range $-0.2\,\text{V} \leqslant E \leqslant 0.018$ V, but it diminishes abruptly for $E > 0.018$ V (Fig. 3(b)).

3.2.4. Ni in AA-containing aqueous 0.5 M H_2SO_4. The inhibition of nickel corrosion in AA-containing aqueous 0.5 M H_2SO_4 depends on c_{AA}, as concluded from the corresponding anodic stripping voltammograms and current transients.

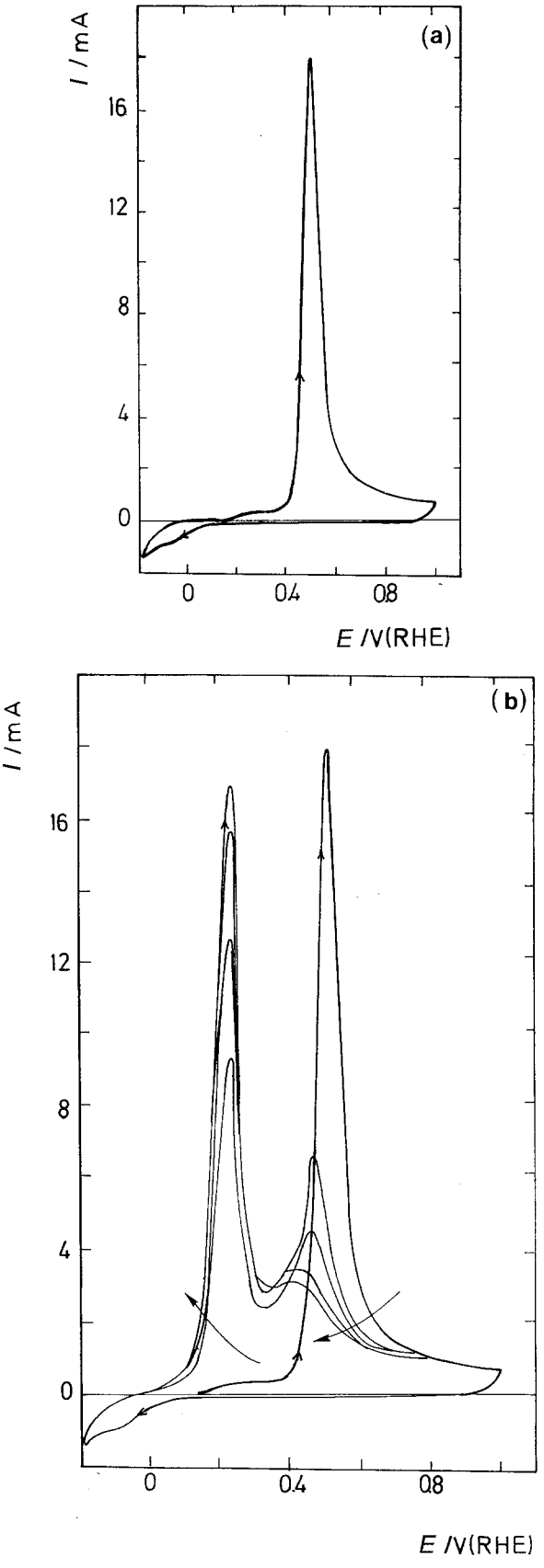

Fig. 2. (a) Voltammogram for Ni in the blank after Ni immersion in CO-saturated aqueous 0.5 M H_2SO_4 for 5 min, at 0 V. $v = 0.1$ V s^{-1}, $T = 25$ °C. (b) Cyclic voltammograms for Ni in the blank after Ni immersion in CO-saturated aqueous 0.5 M H_2SO_4 for 5 min, at 0 V, $v = 0.1$ V s^{-1}, $T = 25$ °C. Arrows indicate the direction of voltammetric profile variations. The potential sweep direction is indicated by arrows on the voltammograms.

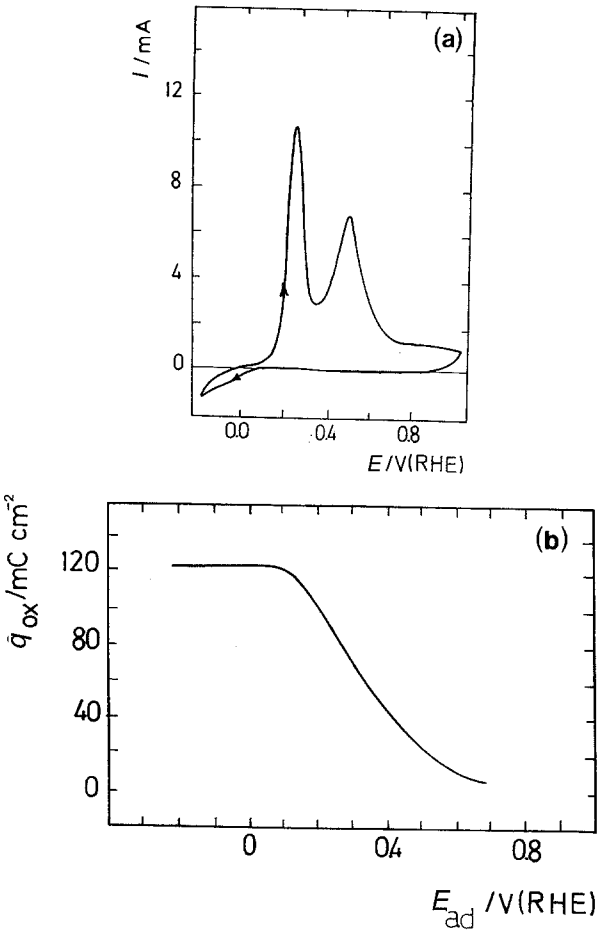

Fig. 3. (a) Voltammogram for Ni in the blank after Ni immersion in ET-saturated aqueous 0.5 M H_2SO_4 for 5 min, at 0 V, $v = 0.1\,V\,s^{-1}$, $T = 25\,°C$. (b) q_{ox} against E_{ad} plot resulting from voltammograms for Ni run in the blank after Ni immersion in ET-saturated aqueous 0.5 M H_2SO_4 for 5 min, at different E_{ad}, $v = 0.1\,V\,s^{-1}$, $T = 25\,°C$. The potential sweep direction is indicated by arrows on the voltammograms.

For a nickel electrode which has been kept in AA-containing solution ($7 \times 10^{-3} < c_{AA} < 0.1$ M) for 5 min, at $E = 0$ V, the nickel electrodissolution process is inhibited. In fact, the corresponding voltammogram in the blank (Fig. 4(a)) shows a decrease in the height of peak I, and simultaneously the appearance of a new peak at 0.48 V. The value $q_{ox} = 59\,mC\,cm^{-2}$ is derived from this type of experiment. Otherwise, when the same run is made for $c_{AA} = 1.7 \times 10^{-2}$ M. The voltammogram shows peak I considerably reduced, and simultaneously the new peak is shifted from 0.48 to 0.54 V (Fig. 4(b)). The value of q_{ox} is then reduced to $44\,mC\,cm^{-2}$.

For nickel previously held in AA-containing solution, the value of q_{ox} resulting from the voltammogram run in the blank also depends on E_{ad} and it reaches a maximum value of q_{ox} for $E = E_{rest}$. From the comparison of q_{ox} values at $c_{AA} = c_{ET}$, it results that the nickel electrodissolution inhibition in AA containing solution is greater than in ET-containing solution.

For nickel immersed in the blank, current transients (Fig. 5(a) and (b)) were run at $E = -0.038$ V and $E = 0.105$ V with AA addition at a certain time. For $E = -0.038$ V, the current transient shows a

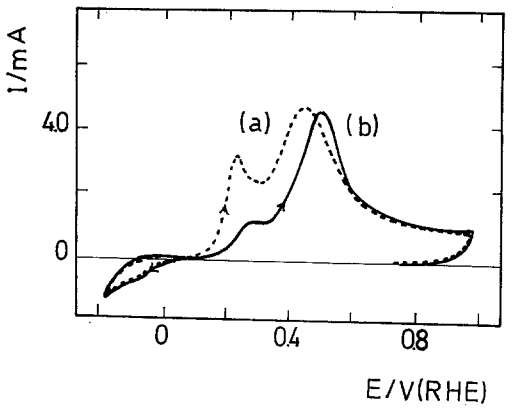

Fig. 4. Voltammograms for Ni in the blank after Ni immersion in AA-containing aqueous 0.5 M H_2SO_4 for 5 min, at 0 V, $v = 0.1\,V\,s^{-1}$. (a) 7×10^{-3} M AA aqueous 0.5 M H_2SO_4; (b) 1.7×10^{-2} M AA aqueous 0.5 M H_2SO_4 at $T = 25\,°C$. The potential sweep direction is indicated by arrows on the voltammograms.

fluctuating cathodic current followed by a smooth decay to a constant electroreduction current. This current increases with c_{AA}. Voltammograms subsequently run from either $E = -0.038$ V or $E = 0.105$ to 1.0 V are qualitatively similar to those illustrated in Fig. 4(a) and (b).

On the other hand, the current transient run at $E = 0.105$ V displays an anodic current maximum followed by a relatively fast decay to null current after 300 s (Fig. 5(b)). The voltammogram run in the positive potential direction is rather different from that seen in Fig. 5(a), as it displays a single main peak at about 0.5 V.

3.2.5. Ni in AC-saturated aqueous 0.5 M H_2SO_4. Current transients of nickel in AC-saturated ($c_{AC} = 0.44$ M) solution at $E_{ad} = -0.038$ V show a negligible cathodic current. The same run made for $E_{rest} = 0.288$ V shows a remarkable inhibition of nickel electrodissolution caused by the presence of AC.

It appears that products from the interaction of nickel with AC at 0 V, inhibit drastically nickel electrodissolution (Fig. 6(a)). In this case, an anodic current can be observed only for $E > 0.4$ V. A subsequent voltammogram run in the positive

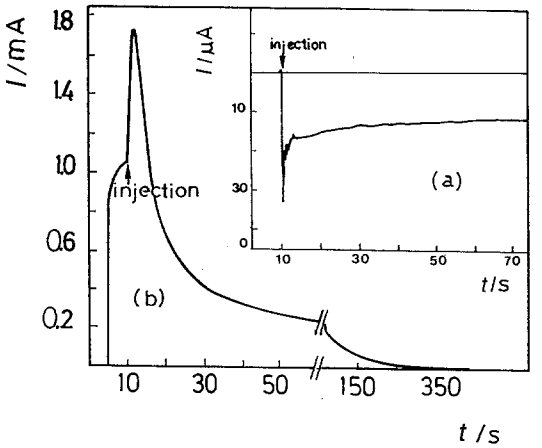

Fig. 5. Current transients measured for Ni in the blank with AA-injection. (a) $E = -0.039$ V; (b) $E = 0.105$ V at $T = 25\,°C$.

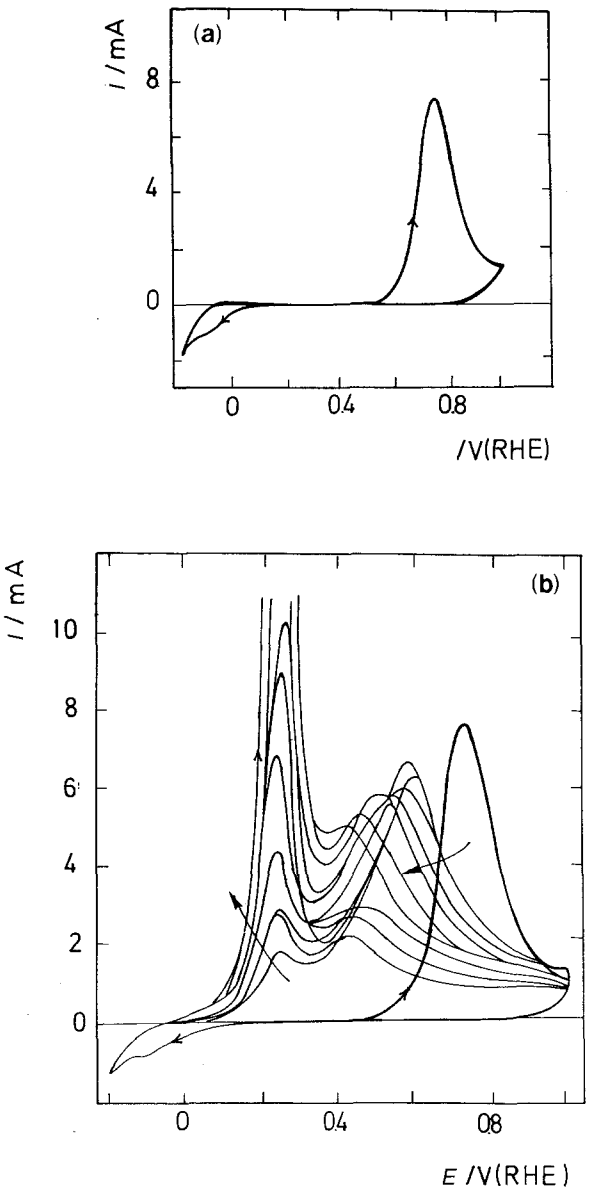

Fig. 6. (a) Voltammogram for Ni in the blank after Ni immersion in AC-saturated aqueous 0.5 M H_2SO_4 for 5 min, at 0 V. $v = 0.1\,V\,s^{-1}$ at $T = 25\,°C$. (b) Cyclic voltammograms for Ni in the blank after Ni immersion in AC-saturated aqueous 0.5 M H_2SO_4 for 5 min, at 0 V; $v = 0.1\,V\,s^{-1}$ at $T = 25\,°C$. Arrows indicate the direction of voltammetric profile variations. The potential sweep direction is indicated by arrows on the voltammograms.

potential direction exhibits an asymmetric peak at 0.74 V, whereas the reverse scan is comparable to that of the blank (Fig. 1(a)). The value $q_{ox} = 42\,mC\,cm^{-2}$ is nearly constant in the range $-0.2\,V \leqslant E \leqslant 0.288\,V$, but it diminishes for $E > 0.3\,V$.

Nickel specimens which have been kept in contact with an AC-containing solution for 5 min, can be activated progressively in the blank by cyclovoltammetry between −0.2 and 1 V at $0.1\,V\,s^{-1}$ (Fig. 6(b)).

3.2.6. Ni in PA-containing aqueous 0.5 M H_2SO_4. The current transient resulting from the addition of PA to the blank ($c_{PA} = 0.44$ M), at $E = 0.278$ V, shows that nickel electrodissolution current decreases abruptly to zero (Fig. 7(a)) as for AC, although nickel electrodissolution inhibition caused by PA increases with c_{PA} (Fig. 7(b)).

For $E = 0$ V and $c_{PA} = 1.25 \times 10^{-4}$ M, the positive-going potential voltammogram becomes similar to that of the blank, but for $c_{PA} = 5 \times 10^{-4}$ M, a drastic decrease in the height of peak I, and a new peak at about 0.6 V are observed (Fig. 7(b)). Moreover, for $c_{PA} \simeq c_{AC} = 0.44$ M, both systems behave rather similarly, except that for PA the potential of the new peak is shifted negatively as compared to that recorded after nickel interaction with the AC-containing solution.

After the interaction with PA-containing solutions, the voltammetric characteristics of nickel in the blank can be recovered by cyclovoltammetry (see Section 3.5). For PA-containing solution the complete reactivation of nickel is achieved after only 12 cycles.

3.3. *Stationary potentiostatic polarization data on additive-containing aqueous 0.5 M H_2SO_4*

Values of E_{corr} and j_{corr} (Table 2) were determined from potentiostatic polarization curves, plotted as potential against $\log j$ (Fig. 8) where j stands for the apparent current density. The additive in the solution changes the value of both E_{corr} and j_{corr} as compared to the blank. For ET and diluted AA-containing solutions, j_{corr} decreases in almost one order of

Table 2. E_{corr}, j_{corr}, b_a and b_c values obtained from Ni pc in aqueous 0.5 M H_2SO_4 containing the different additives at 25 °C

System	E_{corr}/V	j_{corr}/A cm^{-2}	b_a/V decade^{-1}	$-b_c$/V decade^{-1}
Ni/0.5 M H_2SO_4	−0.020	1.4×10^{-3}	0.060	0.120
Ni/(ET) 0.5 M H_2SO_4	−0.005	8.0×10^{-4}	0.060	0.090
Ni/(AA 7×10^{-3} M) 0.5 M H_2SO_4	0.065	1.3×10^{-4}	0.066	0.090
Ni/(AA 10^{-1} M) 0.5 M H_2SO_4	0.100	2.1×10^{-5}	0.060*, 0.040†	0.090
Ni/(CO) 0.5 M H_2SO_4	0	1.0×10^{-6}	0.060	0.090
Ni/(PA 5×10^{-3} M) 0.5 M H_2SO_4	0.225	8.1×10^{-6}	0.030	0.225
Ni/(PA 4.4×10^{-2} M) 0.5 M H_2SO_4	0.260	1.9×10^{-6}	0.030	0.230
Ni/(AC) 0.5 M H_2SO_4	0.320	1.5×10^{-7}	0.030	0.200

* For potentials close to E_{corr}.
† For potentials far from E_{corr}.

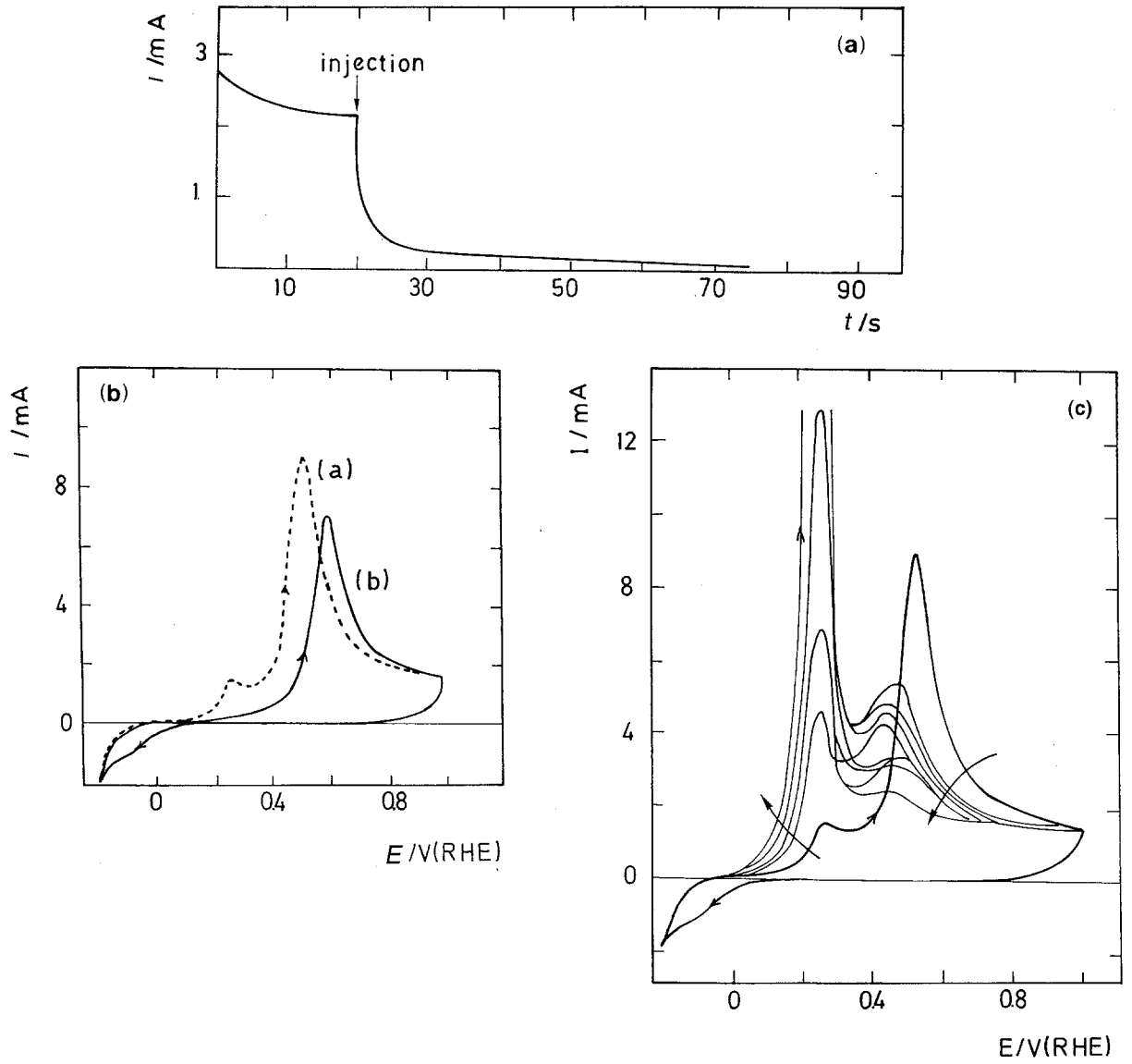

Fig. 7. (a) Current transient measured for Ni in the blank with PA-injection. $E = 0.278$ V at $T = 25$ °C. (b) Voltammograms for Ni in the blank after Ni immersion in PA-containing aqueous 0.5 M H_2SO_4 for 5 min at 0 V, $v = 0.1\ V\ s^{-1}$, $T = 25$ °C: (a) 5×10^{-4} M PA aqueous 0.5 M H_2SO_4; (b) 0.44 M PA aqueous 0.5 H_2SO_4, $T = 25$ °C. (c) Cyclic voltammograms for Ni in the blank after Ni immersion in 0.44 M PA aqueous 0.5 M H_2SO_4 for 5 min, at 0 V. $v = 0.1\ V\ s^{-1}$, $T = 25$ °C. Arrows indicate the direction of voltammetric profile variations. The potential sweep direction is indicated by arrows on the voltammograms.

magnitude, whereas for $c_{AA} > 0.1$ M, CO, PA and AC-containing solutions, lower values of j_{corr} are obtained. On the other hand, E_{corr} shifts positively in additive-containing solution, the largest shift being produced by triple C–C bond containing additives.

For $E \gg E_{corr}$, and $E \ll E_{corr}$, the nickel electrodissolution and HER, respectively, exhibit a Tafel relationship in all solutions.

The anodic Tafel slope, $b_a \simeq 2.3RT/F$, is confirmed for nickel in the blank as well as in those solutions containing CO and ET under saturation, and diluted AA, whereas for $c_{AA} > 0.1$ M, two anodic Tafel regions are found with slopes $b_a \simeq 2.3RT/F$ for $E \simeq E_{corr}$, and $b_a \simeq 2.3(2RT/3F)$ for $E \gg E_{corr}$. Otherwise, a triple C–C bond additive in the solution decreases b_a from $2.3RT/F$ to almost $2.3RT/2F$.

The cathodic Tafel slope resulting from the blank is $b_c \simeq -2.3(2RT/F)$, whereas $b \simeq -2.3(3RT/2F)$ in ET, AA or CO-containing solution, and it rises to $b_c \simeq -2.3(4RT/F)$ for AC and PA-containing solution (Table 2). The influence of additives with a C–C triple bond on the HER confirms data already reported in the literature [13].

3.4. *Chemical analysis data*

The amount of dissolved Ni was determined by atomic absorption spectroscopy after holding nickel for 15 min in the range $0.25\ V \leqslant E \leqslant 0.75\ V$ in either the blank or additive-containing solution. Data are assembled in Table 3. For all values of E, the amount of soluble Ni decreases in the order ET > AA > CO > PA > AC.

4. Analysis of voltammograms

Based upon the earlier proposed mechanism for the nickel electrodissolution [14 and references therein] and considering Temkin-type adsorption isotherm

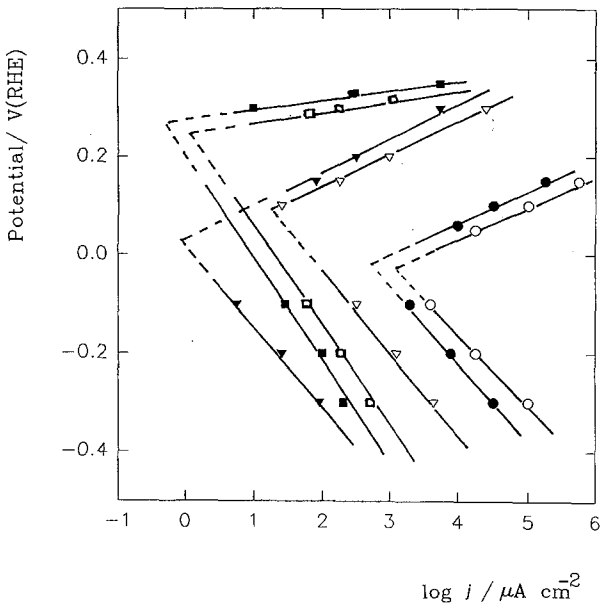

Fig. 8. Anodic and cathodic Tafel plots for Ni in the blank and in additive-containing aqueous 0.5 M H_2SO_4 at 25 °C. (○) Ni/0.5 M H_2SO_4, (●) Ni/(ET_{sat}) 0.5 M H_2SO_4, (△) Ni/0.1 M AA in 0.5 M H_2SO_4, (□) Ni/0.44 M PA in 0.5 M H_2SO_4 (■) Ni/(AC_{sat}) 0.5 M H_2SO_4 and (▲) Ni/(CO_{sat}) 0.5 M H_2SO_4.

conditions for the species involved in the various surface processes [4, 9], the following general expression was used for j_a, the anodic current density in the voltammogram,

$$j_a = k_i^{0\prime}\theta_i \exp\left[\frac{\alpha F(E - E_i^{0\prime})}{RT}\right] \exp[r_i\theta_i] \qquad (1)$$

where $k_i^{0\prime}$ is the formal chemical rate constant of the ith-reaction, θ_i is the degree of surface coverage by ith-species, α is the anodic transfer coefficient assisting the electrochemical reaction in the anodic direction, $E_i^{0\prime}$ is the formal standard potential, and r_i stands for the variation of the electrochemical adsorption free energy with θ_i, at constant temperature (T). The use of the rate equation (Equation 1) can be justified by previous work on the electrochemical behaviour of nickel in aqueous aggressive environments [14] including the validity of Temkin-type adsorption conditions [4, 9].

For a linear potential sweep run in the positive potential direction,

$$E = E_s + vt \qquad (2)$$

where E_s is the potential at which the sweep commences at the potential sweep rate, v. For a surface electrochemical reaction, j_a can be expressed as

$$j = -K_{Mi}\left(\frac{d\theta_i}{dt}\right)_T \qquad (3)$$

where K_{Mi} represents a reference charge density related to the complete coverage of the nickel surface by the ith-species and the sign accounts for the decrease in θ_i during the anodic potential sweep. Then, from Equations 1, 2 and 3, it follows that

$$\theta_i = \frac{1}{1 - r_i}\left[\theta_i^0 - \frac{\bar{k}_i^{0\prime}RT}{K_{Mi}\alpha vF}\right] \exp\left(\frac{\alpha F(E - E_s)}{RT}\right) \qquad (4)$$

where θ_i^0 is the initial surface coverage by ith-species, and $\bar{k}_i^{0\prime}$ is a formal electrochemical rate constant, that is,

$$\bar{k}_i^{0\prime} = k_i^{0\prime} \exp\left(\frac{-\alpha FE_i^{0\prime}}{RT}\right) \qquad (5)$$

Equations 1 and 3 can be solved by conventional methods [15] using Equation 4. Correspondingly, for the simulation of voltammograms the following fitting parameters were tested, θ_i, r_i, C and D, where $C \equiv RT/\alpha F$ and $D \equiv -(\bar{k}_i^{0\prime}/K_{Mi}v)$. Simulated voltammograms for the different systems are shown in Fig. 9(a–f), and both, fitting parameters and kinetic data derived for each system, are assembled in Table 4. It should be noted that deconvolution data have to be handled carefully, particularly when the potential of the peaks varies due to the change in the relative degree of surface coverage by different adsorbates.

5. Interpretation and discussion

The electrochemical behaviour of nickel in aqueous 0.5 M H_2SO_4 within the active to passive transition potential range has been described by three main contributions, namely, the electrodissolution of nickel yielding soluble Ni(II) species, the electroformation of the anodic layer, which includes the appearance of $Ni(OH)_2$, NiO and passivating species, and the chemical dissolution of the anodic layer [16–20].

The anodic processes related to peak A_1 involve a consecutive reaction pathway which can be put

Table 3. Concentration of dissolved Ni resulting after holding a Ni pc electrode at different potentials for 15 min

System	c_{Ni}^{2+}/mg dm^{-3} $E = 0.25$ V	c_{Ni}^{2+}/mg dm^{-3} $E = 0.50$ V	c_{Ni}^{2+}/mg dm^{-3} $E = 0.80$ V
Ni/0.5 M H_2SO_4	26	1	1
Ni/(ET_{sat}) 0.5 M H_2SO_4	23	1	1
Ni/(CO_{sat}) 0.5 M H_2SO_4	2	2	2
Ni/(0.10 M AA) 0.5 M H_2SO_4	5	3	3
Ni/(0.44 M PA) 0.5 M H_2SO_4	2	3	3
Ni(AC_{sat}) 0.5 M H_2SO_4	1	2	1

Table 4. Parameters resulting from voltammogram deconvolution in aqueous 0.5 M H_2SO_4 after Ni immersion in additive-containing solutions

Voltammetric peak	E_p/V	$I_p \times 10^3$/A	θ_p	q_{ox}/mC cm^{-2}	$\bar{k}_i^{0\prime}$/cm s^{-1}
Ni/0.5 M H_2SO_4					
Peak A_1	0.22	9.72	0.86	24.8	5.7×10^{-2}
Peak A_2	0.43	1.30	0.09	6.0	1.2×10^{-4}
Ni/(CO_{sat})0.5 M H_2SO_4					
Peak B_1	0.27	0.38	0.03	10.5	5.0×10^{-2}
Peak B_2	0.51	14.30	0.95	40.6	8.3×10^{-5}
Peak B_3	0.58	0.73	0.06	4.5	3.1×10^{-5}
Ni/(ET_{sat}) 0.5 M H_2SO_4					
Peak C_1	0.25	9.06	0.81	24.0	4.5×10^{-2}
Peak C_2	–	1.26	0.18	12.0	–
Peak C_3	0.49	4.66	0.22	18.0	1.4×10^{-7}
Ni/(7×10^{-3} M AA) 0.5 M H_2SO_4					
Peak D_1	0.27	1.96	0.13	7.5	1.1×10^{-2}
Peak D_2	0.29	0.57	0.02	0.7	1.0×10^{-5}
Peak D_3	0.46	2.90	0.20	13.5	6.4×10^{-5}
Peak D_4	0.47	0.94	0.08	6.8	1.6×10^{-7}
Ni/(AC_{sat}) 0.5 M H_2SO_4					
Peak E_1	0.75	3.22	0.16	13.3	1.0×10^{-10}
Peak E_2	0.76	2.72	0.17	13.0	2.9×10^{-11}
Ni/(4.4×10^{-2} M PA) 0.5 M H_2SO_4					
Peak F_1	0.65	4.71	0.24	10.3	1.3×10^{-9}
Peak F_2	0.65	2.57	0.14	12.0	1.7×10^{-9}
Peak F_3	0.73	1.00	0.05	2.2	3.2×10^{-10}

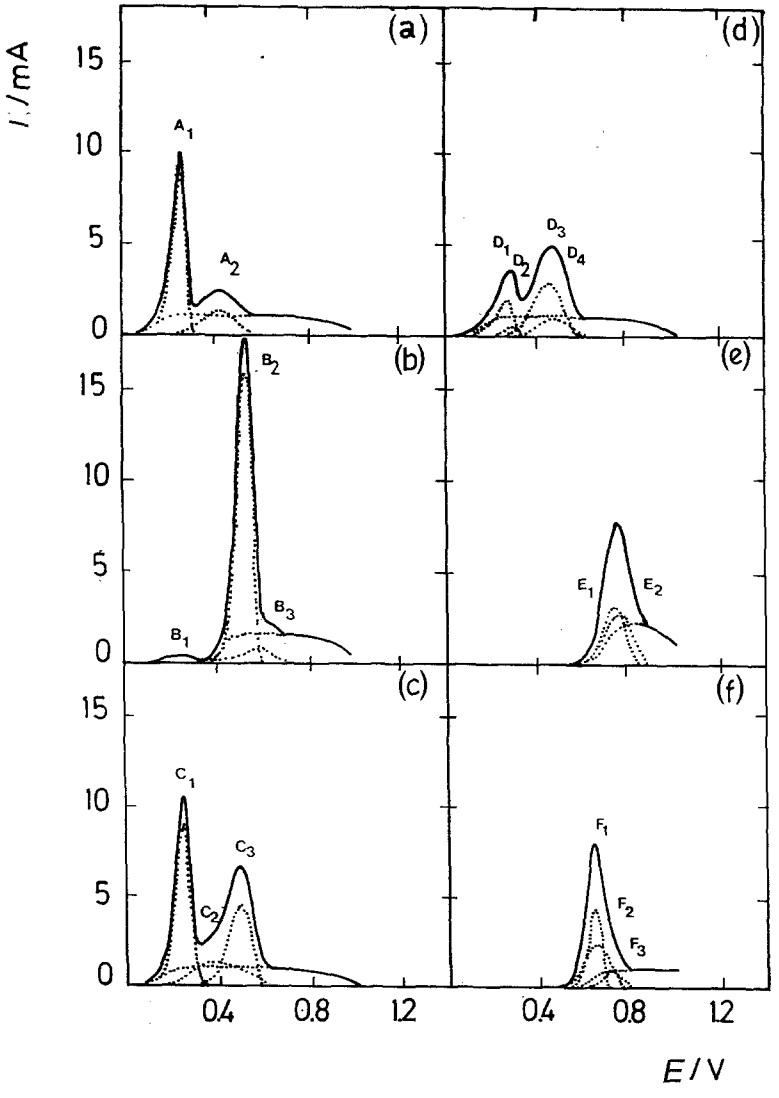

Fig. 9. Deconvolution of voltammograms run in the positive potential direction. (a) Ni/0.5 M H_2SO_4, (b) Ni/(CO_{sat}) 0.5 M H_2SO_4, (c) Ni/(ET_{sat}) 0.5 M H_2SO_4, (d) Ni/7×10^{-3} M AA in 0.5 M H_2SO_4, (e) Ni/(AC_{sat}) 0.5 M H_2SO_4, (f) Ni/0.44 M PA in 0.5 M H_2SO_4. Full lines represent overall voltammograms.

forward as follows:

$$[Ni(H_2O)_{ad}] = [Ni(OH)_{ad}] + H^+ + e^- \quad (6a)$$

$$[Ni(OH)_{ad}] = [Ni(OH)_{ad}]^+ + e^- \quad (6b)$$

$$[Ni(OH)_{ad}]^+ + H_2O = \{Ni(OH)_2\} + H^+ \quad (6c)$$

and the Ni^{2+} ion formation from the OH-adsorbed species implies reactions such as

$$[Ni(OH)_{ad}] + H^+ = Ni^{2+} + H_2O \quad (6d)$$

$$\{Ni(OH)_2\} + 2H^+ = Ni^{2+} + 2H_2O \quad (6e)$$

The anodic processes responsible for peak A_2 can also be described by a complex reaction pathway in the following way:

$$\{Ni(OH)_2\} + H_2O = \{Ni(OH)_2 \cdot H_2O\} \quad (7a)$$

$$3[Ni(OH)_{ad}] = [2Ni(OH)_{ad} \cdot Ni(OH)^+_{ad}] + e^- \quad (7b)$$

leading to the electroformation of the anodic layer from reaction (6(a)–(c)) and (7(a)–(b)).

Finally, the partial chemical dissolution of the oxide layer can be represented by the following reaction:

$$[2Ni(OH)_{ad} \cdot Ni(OH)^+_{ad}] + H^+ = \{Ni \cdot Ni(OH)_2\} + Ni^{2+} + H_2O \quad (8)$$

On the other hand, the spontaneous corrosion of nickel in an acid environment is accompanied by the HER as the main cathodic process. The HER on nickel in the blank fits a Tafel relationship with $b_c = -2.3(2RT/F)$ and $j_0 = 10^{-5.22}\,A\,cm^{-2}$, in agreement with data already reported in the literature [21]. A further analysis of kinetic data related to the HER indicates that an electrochemical desorption probably determines the rate of the HER on Ni in acid.

The comparison between the simulated (Fig. 9(a)) and experimental data (Fig. 1) allowed us to estimate the relative contribution of reactions (6(a)–(e)) (peak A_1 at 0.22 V), and reactions (6(a)–(c)) and (7(a)–(b)) (peak A_2 at 0.43 V), followed by Ni passivation. The formal rate constants derived for each voltammetric peak are assembled in Table 3.

5.1. *Influence of CO*

The bonding of CO to Ni proceeds by donation of the lone pair of electrons of the carbon atom to vacant d orbitals of Ni. For this interaction, the electro-donation capability of CO is small and a back-donation of electrons from filled d orbitals of Ni to vacant π^* antibonding orbitals of CO is favoured.

The CO interaction with nickel in the electrochemical environment produces an abrupt decrease in the height of peak A_1 (Fig. 2), but the lack of a current transient at a constant E, as CO is added to aqueous 0.5 M H_2SO_4 indicates that in this case nickel electrodissolution is strongly inhibited presumably by the presence of CO-adsorbates. In fact, a small amount of soluble nickel species at 0.25 V determined by AAS (atomic absorption spectroscopy) can still be found in the presence of CO (Table 2) [4].

The anodic electrodissolution of nickel in the presence of CO can be interpreted as a series of reaction such as:

$$[Ni(H_2O)]_{ad} + CO_{(aq)} = [Ni(CO)_{ad}] + H_2O \quad (9a)$$

$$[(Ni(H_2O)_{ad}] = [Ni(OH)_{ad}] + H^+ + e^- \quad (9b)$$

Accordingly, in the presence of CO adsorbates only a fraction of the nickel surface would be available for nickel electrodissolution following the reaction pathway (6(a)–(e)). In this case, the voltammogram simulation (Fig. 9b) comprises three main current contributions related to peaks B_1, B_2 and B_3. The potential of peak B_1 is similar to that resulting from the blank (peak A_1 in Table 2). Likewise, the value of $\bar{k}_1^{0\prime} \simeq 5 \times 10^{-2}\,cm\,s^{-1}$ is very close to that of the blank. This means that at CO free Ni sites, the conventional kinetics of the nickel electrodissolution is observed.

On the other hand, peak B_2 located at 0.5 V can be assigned to the CO electrooxidative desorption and simultaneous $[Ni(OH)]_{ad}$ formation, because the amount of soluble nickel found at this potential, that is, a potential at which the nickel surface is still largely covered by CO-adsorbates, becomes very low as compared to that of the blank.

The electrooxidative desorption of CO, which can be represented as

$$[Ni(CO)_{ad}] + 2H_2O = CO_2 + [Ni(OH)_{ad}] + 3H^+ + e^- \quad (9c)$$

is subsequently followed by Ni^{2+} ion electroformation and the electrooxidation of $[Ni(OH)_{ad}]$ to $\{Ni(OH)_2\}$ leading to the appearance of peak B_3 (Table 4) [1, 2].

In agreement with the preceding description, potentiostatic polarization data (Table 2) indicate that the value of b_a remains the same as that for nickel in the blank, whereas in the presence of CO $b_c \simeq -2.3(3RT/2F)$. This decrease in b_c might be caused by a change in the adsorbate–adsorbate interactions, although this is far from proven. The above explanation is consistent with the fact that the rate of nickel electrodissolution in CO-containing solution is three orders of magnitude lower than in the blank. The presence of CO delays, therefore, both nickel electrodissolution and the HER [5].

5.2. *Influence of ET*

The molecular adsorption of ET is accomplished by a π-bonding interaction which involves a charge donation from the ethylene molecule to d orbitals of Ni, and in some cases, a charge back-donation to the ethylene π^* antibonding orbitals [22].

Potentiostatic current transients indicate that molecular ET adsorption on nickel from the electrochemical environment is likely. In fact, no electroadsorption current can be detected in the range $-0.1\,V \leqslant E \leqslant 0.4\,V$.

The simulation of the anodic voltammogram after ET interaction with nickel (Fig. 9(c)) shows peak C_1 at 0.25 V, which resembles peak A_1 in the blank (Table 4), peak C_2 at about 0.4 V, and peak C_3 at about 0.5 V. Peak C_2 involving $q_{ox} \simeq 12\,mC\,cm^{-2}$, can probably be attributed to ET electrodesorption from the nickel corroding surface. The presence of an ET-adsorbate would produce a decrease in the formal rate constant of $\{Ni(OH)_2\}$ and $\{NiO\}$ formation, a process which can be assigned to peak C_3.

The relatively little influence of ET on nickel electrodissolution is consistent with the similar amount of soluble nickel detected and the small voltammetric changes observed in this system as compared to the blank (Fig. 3(a)). Moreover, potentiostatic polarization curves for the nickel in the ET-containing solution show anodic and cathodic Tafel lines similar to those found for the blank. Nevertheless, the nickel electrodissolution rate is only one order lower than in the blank.

5.3. *Influence of AA*

Seemingly, the interaction of AA with nickel is comparable to that of AA with Pt, that is, it can be explained as a π bonding between the double C–C bond and d orbitals of Ni, as it was concluded by EELS (electron energy loss spectrometry) and AES (Auger electron spectroscopy) [23]. Molecular models favour a double C–C bond parallel to the metal surface, so that the $-CH_2OH$ group extends away from the plane. Otherwise, it has been shown that AA-electroadsorption on Pt(1 1 1) yields CO and olefinic residues, which were detected by EELS and FTIRS (Fourier transform infrared spectroscopy) [23].

The voltammogram deconvolution resulting after Ni-AA interaction at $E = 0\,V$ for $c_{AA} = 7 \times 10^{-3}\,M$ AA, consists of four main contributions, namely, peak D_1 at 0.27 V which can be related to nickel electrodissolution and $\{Ni(OH)_2\}$ formation, peaks D_2 and D_3 which can be attributed to the anodic stripping of distinguishable organic residues formed from AA adsorption, and peak D_4 probably related to $\{Ni(OH)_2\}$ dissolution and $\{NiO\}$ formation. The height of peak D_1 decreases as c_{AA} is increased. Peak D_1 can be related to nickel electrodissolution itself. Peak D_2 can be related to the desorption of CO-type residues, as the corresponding formal rate constant derived from this peak is similar to that attributed to peak B_2 for the CO-containing solution, although D_2 is shifted negatively 0.3 V as compared to peak B_2, probably because of the lower CO residue surface coverage resulting from AA dissociative adsorption. Correspondingly, peak D_3 can be attributed to the electrooxidation of the olefinic-adsorbate fraction.

For AA-containing solutions a considerable positive potential shift of E_{corr} is observed on increasing c_{AA} (Table 2). Besides, for $E \simeq E_{corr}$, it results in $b_a \simeq 2.3RT/F$, but for $E \gg E_{corr}$ and $c_{AA} > 0.1\,M$, $b_a \simeq 2.3(2RT/3F)$. Otherwise, for $c_{AA} = 0.1\,M$ it results in $b_c \simeq -2.3(3RT/2F)$, that is, the same value of b_c as that found in CO and ET-containing solutions.

5.4. *Influence of AC*

Several structures for metal-alkyne complexes are consistent with the Dewar–Chatt–Duncanson scheme of bonding [24]. EELS studies have shown that AC molecular adsorption on Ni(1 1 1) takes place at room temperature, but dissociative adsorption involving several hydrocarbon fragments can be observed on heating to higher temperatures [25, 26]. The great extent of back-donation of electrons from Ni to AC, causes a strong Ni–C covalent bond and, therefore, a weaker and more elongated triple C–C bond can result [27, 28].

The voltammogram simulation after Ni–AC interaction in the electrochemical environment exhibits two main current contributions, namely, peaks E_1 and E_2 both at about 0.75 V. Peak E_1 can be assigned to the AC-residue electrooxidation, and peak E_2 to the $\{Ni(OH)_2\}$ electrodissolution and $\{NiO\}$ formation. It should be noted, however, that the potential of E_2 is positively shifted with respect to that of peak A_2 in the blank. This shift indicates that Ni electrodissolution in AC-containing solutions is strongly inhibited by adsorbate formation. This would mean that a competitive adsorption, such as

$$[Ni(OH)_{ad}] + AC = [Ni(AC)_{ad}] + OH^- + H^+ \quad (10)$$

is totally displaced to the right as can be envisaged from the voltammogram (Fig. 6(a)), the value of E_{corr}, and the low value of j_{corr}.

5.5. *Influence of PA*

The inhibition of PA for metal dissolution can be explained through an initial interaction of the triple C–C bond with the metal surface. The EELS spectrum of PA-adsorbates on Pt in aqueous solution shows a double C–C bond stretching frequency instead of that corresponding to a triple C–C bond [23], that is, the adsorption of PA on Pt lowers the bond order of the unsaturated C–C bond. CO and hydrocarbon species have been found [23] as adsorbed residues on platinum from diluted aqueous solution when $E_{ad} \simeq 0.4\,V$. Taking into account that the bonding of adsorbates on nickel is to some extent comparable to the bonding of adsorbates on platinum [29], the adsorption of PA on nickel would lead to a disrupture of the molecule yielding, at least, two distinguishable adsorbate moieties.

Voltammetric data on nickel electrodissolution

after interaction with the PA-containing solution show a stronger inhibition of the anodic reactions than in other olefinic species-containing solution, but weaker than that produced by AC-residues. Furthermore, nickel reactivation in the blank after interacting with the PA-containing solution by repetitive potential cycling requires a lower number of cycles than for the AC-containing solution.

In contrast to AA, PA is adsorbed on nickel through a chemical reaction, therefore, no anodic superimposed current is recorded during the current transient after PA injection to the blank.

The voltammogram simulation resulting from nickel after immersion in the 0.44 M PA-containing solution at $E = 0$ V for 5 min, involves three main contributions. Assuming that a dissociative adsorption of PA takes place on nickel as it does for platinum [23], at least CO-type and hydrocarbon residues would be formed. Then, peak F_1 would be mainly related to the electrooxidation of CO-type residues. Peak F_1 is shifted positively as compared to peak B_2 for the CO-containing solution. Otherwise, peak F_2 can be mainly assigned to the electrooxidation of hydrocarbon residues and peak F_3 to $\{Ni(OH)_2\}$ electrodissolution and $\{NiO\}$ formation.

The Tafel slope for the HER on Ni in the presence of AC and PA is $b_c \simeq -2.3(4RT/F)$. This indicates that the reaction involves a large cathodic polarization, presumably caused by hydrocarbon-type and CO-type residues completely covering the nickel surface. Conversely, the value of b_a decreases from $2.3RT/F$ to $2.3(2RT/3F)$. This decrease in b_a is similar to that reported for some other hydrocarbon electrooxidations on platinum [30]. Seemingly, the presence of PA in the acid solution favours in this case PA electrooxidation rather than nickel electrodissolution at least in the range of potential $0.3 \leqslant E \leqslant 0.6$ V.

6. Conclusions

(i) The influence of several foreign substances on the nickel electrooxidation and HER in aqueous 0.5 M H_2SO_4 was investigated by stationary polarization curves, anodic single sweep voltammetry after Ni-foreign substance interaction, and current transients at a constant potential with the injection of the foreign substance to the acid.

The deconvolution voltammograms resulting from nickel in the blank after interacting with a foreign substance-containing solution becomes useful to envisage the effect of those substances on nickel electrooxidation.

(ii) The greatest inhibition of nickel electrodissolution in acid is caused by organic compounds involving a C–C triple bond, such as acetylene and propargyl alcohol.

(iii) Organic substances with a double C–C bond tend to produce a lower inhibition of nickel electrooxidation than those with a triple C–C bond. Allyl alcohol becomes more effective than ET because of its disruptive electroadsorption leading to CO-type and olefinic adsorbed species on nickel.

(iv) Ni electrodissolution inhibition caused by the presence of carbon monoxide is greater than that resulting from double and triple C–C bond compounds at the same concentration in the acid.

Acknowledgements

This work was financially supported by the Consejo Nacional de Investigaciones Científicas y Técnicas (CONICET) of Argentina. A.M.C.L. is a member of the research career at the Comisión de Investigaciones Científicas de la Pcia. de Bs. As. (CIC). C.F.Z. is a member of the Program de Desarrollo de Ciencias Básicas (PEDECIBA). Uruguay. Authors thank R. Iasi from CIDEPINT for his collaboration in AAS analyses.

References

[1] J. R. Vilche and A. J. Arvia, *in* 'Passivity of Metals', (edited by R. P. Frankenhal and J. Kruger), The Electrochemical Society, Corrosion, Monographs Series, Princeton, NJ (1978), p. 861.
[2] M. R. Barbosa, S. G. Real, J. R. Vilche and A. J. Arvia, *J. Electrochem. Soc.* **135** (1988) 1977.
[3] D. W. McKee and M. S. Pak, *ibid.* **116** (1969) 516.
[4] A. M. Castro Luna and A. J. Arvia, *J. Appl. Electrochem.* **21** (1991) 435.
[5] A. T. Skyarov and Ya M. Kolotyrkin, *Elektrokhimiya* **1** (1965) 3.
[6] A. B. Delgado, A. M. Castro Luna, W. E. Triaca and A. J. Arvia, *J. Electrochem. Soc.* **129** (1982) 1493.
[7] D. Zurawszi, K. Chan and A. Wieckowski, *J. Electroanal. Chem.* **210** (1986) 315 and **230** (1987) 205.
[8] M. C. Arevalo, A. M. Castro Luna, A. Arevalo and A. J. Arvia, *ibid.* **330** (1992) 595.
[9] A. Wieckowski, S. D. Rosasco, G. N. Salaita, A. T. Hubbard, B. E. Bent, F. Zaera, D. Godbey and G. A. Somorjai, *J. Amer. Chem. Soc.* **107** (1985) 5910.
[10] E. Pastor and V. Schmidt, Proceedings of the XIth Ibero–American Electrochemical Society Meeting, Aguas de Lindoia, Brazil (1994) p. 96.
[11] G. Brauer, 'Handbuch der Praeparativen Anorganischen Chemie', Part I, Springer Verlag, Stuttgart (1960).
[12] 'International Critical Tables, Vol. 3, National Research Council, McGraw Hill, Chicago (1933), p. 280.
[13] V. Jovancicevic, B. Yang and J. O'M. Bockris, *J. Electrochem. Soc.* **135** (1988) 94.
[14] J. R. Vilche and A. J. Arvia, *Corros. Sci.* **15** (1975) 419 and **18** (1978) 441.
[15] A. D. Booth, *in* 'Numerical Methods', Butterworths, London, 3rd edn (1966).
[16] V. Brusic, *in* 'Oxides and Oxide Films', Vol. I, (edited by J. W. Diggle), Marcel Dekker, New York (1972), p. 1.
[17] A. Visintin, A. C. Chialvo, W. E. Triaca and A. J. Arvia, *J. Electroanal. Chem.* **225** (1987) 227.
[18] J. O'M. Bockris, A. K. N. Reddy and B. Rao, *J. Electrochem. Soc.* **113** (1966) 1133.
[19] V. N. Koutun, V. F. Mogilenko and A. M. Greshik, *Elektrokhimiya* **3** (1974) 25.
[20] P. Marcus and J. M. Herbelin, *Corros. Sci.* **34** (1993) 1123.
[21] J. O'M. Bockris and S. Srinivasan, *Electrochim. Acta* **9** (1964) 31.
[22] X. Y. Zhu and J. M. White, *Surf. Sci.* **214** (1989) 240.
[23] J. Y. Gui, E. Kahn, C.-H. Lin, F. Lu, G. N. Salaita, D. A. Stern, D. C. Zapien and A. T. Hubbard, *J. Electroanal. Chem.* **252** (1988) 169.
[24] G. C. Bond, *in* 'Catalysis by Metals' Academic Press, London (1962) Chapter 12, pp. 281–310.
[25] P. Rudolf, C. Astaldi, S. Modesti and R. Rosei, *Surf. Sci. Lett.* **220** (1989) L714.
[26] Y. Wang and P. Coppers, *Inorg. Chem.* **15** (1976) 1122.

[27] A. Farkas, L. Farkas and E. K. Rideal, *Proc. Roy. Soc. A.* **630** (1934) 146.
[28] O. Beek, *Disc. Faraday Soc.* **8** (1950) 118.
[29] B. Hammer and J. K. Norskov, *Nature* **376** (1995) 238.
[30] J. O'M. Bockris, E. Gileadi and G. Stoner, *J. Phys. Chem.* **73** (1969) 427.